



**HAL**  
open science

# Measurement of Gravel-Bed Topography: Evaluation Study Applying Statistical Roughness Analysis

Stéphane Bertin, H Friedrich

► **To cite this version:**

Stéphane Bertin, H Friedrich. Measurement of Gravel-Bed Topography: Evaluation Study Applying Statistical Roughness Analysis. *Journal of Hydraulic Engineering*, 2014, 140, pp.269 - 279. 10.1061/(asce)hy.1943-7900.0000823 . hal-03470757

**HAL Id: hal-03470757**

**<https://hal.science/hal-03470757>**

Submitted on 21 Dec 2021

**HAL** is a multi-disciplinary open access archive for the deposit and dissemination of scientific research documents, whether they are published or not. The documents may come from teaching and research institutions in France or abroad, or from public or private research centers.

L'archive ouverte pluridisciplinaire **HAL**, est destinée au dépôt et à la diffusion de documents scientifiques de niveau recherche, publiés ou non, émanant des établissements d'enseignement et de recherche français ou étrangers, des laboratoires publics ou privés.

# 1 **Measurement of gravel-bed topography: an evaluation study applying statistical**

## 2 **roughness analysis**

3 S. Bertin<sup>1</sup>; H. Friedrich<sup>2</sup>

4

### 5 **Abstract**

6 In this two-part study, experiments are conducted to evaluate available topography  
7 measurement techniques for gravel-beds in a laboratory flume and to study their suitability for  
8 statistical roughness analysis. The available instruments for this study include, (i) an acoustic  
9 bed-profiler; (ii) a hand-held laser-scanner; and (iii) two digital consumer cameras forming a  
10 stereo-photogrammetric system, and are employed to obtain Digital Elevation Models  
11 (DEMs) of water-worked gravel-beds. In the first part of the study, the three measurement  
12 techniques are reviewed and their feasibilities for future grain-scale roughness work assessed,  
13 based on the obtained elevation datasets. Water-worked gravel-bed topographies are measured  
14 with all three available measurement techniques. The analysis of the DEMs concentrates on  
15 using Probability Distribution Functions (PDFs) and second-order structure functions of bed  
16 elevations. Roughness coefficients are determined and used as a benchmark for comparison of  
17 the three measurement techniques. Although, visually, differences in the DEMs obtained with  
18 different measurement techniques are observed, the results of the chosen statistical analysis do  
19 not disclose the visual differences to the same extent. It is shown that the used stereo-  
20 photogrammetric system, although theoretically allowing a fast and high-resolution recording  
21 process, lacks behind in accuracy. Thus, the second part of the study identifies and presents  
22 steps to improve the quality of the obtained stereo-photogrammetric DEMs. A checklist is

*Page 1*

<sup>1</sup>PhD student, Department of Civil and Environmental Engineering,  
The University of Auckland, Private Bag 92019, Auckland, New Zealand  
\_corresponding author\_ E-mail: sber081@aucklanduni.ac.nz

<sup>2</sup>Lecturer, Department of Civil and Environmental Engineering,  
The University of Auckland, Private Bag 92019, Auckland, New Zealand  
E-mail: h.friedrich@auckland.ac.nz

23 provided, highlighting the improvements made in the follow-up study, in order to obtain a  
24 high-quality stereo-photogrammetric DEM. The overview will be useful for other researchers  
25 to make use of available low-cost and high-quality consumer camera equipment, to set-up  
26 their own, non-proprietary stereo-photogrammetric system.

27

28 **Subject headings:** *Topography; Bed roughness; Distance measurement; Photogrammetry.*

29

## 30 **INTRODUCTION**

### 31 **Roughness characterization**

32 With recent research advances and technology improvement, statistical analysis of bed  
33 elevations in gravel-bed rivers has become crucial to define roughness parameters, quantify  
34 armoring effects, and hence to understand the nature of the river flow.

35 Traditionally, bed-scale roughness parameters used in bedload transport and flow resistance  
36 equations are described using percentiles of the Grain Size Distribution (GSD) of the  
37 sediment constituting the bed. The intermediate particle axis is chosen as the base value for  
38 GSD, despite it is recognized that the short axis is the one protruding into the flow, and is  
39 therefore responsible for the bulk of the resistance to the flow (de Jong 1995; Robert 1990).

40 An equivalent roughness parameter is commonly used, such as Nikuradse's  $k_s$  set to  $3.5D_{84}$ ,  
41 where  $D_{84}$  is the length of the intermediate axis of the sediment particle in the GSD for which  
42 84-% of the particles are smaller (Clifford et al. 1992). GSD characteristics can be determined  
43 with techniques such as sieve analysis, Wolman's (1954) or Fehr's (1987) line-by-number  
44 sampling procedures or similar methods, which require disturbance of the gravel-bed surface.

45 Detailed discussions and comparisons of those methods can be found in the work of Bunte

46 and Abt (2001). 2D image-based automated methods became more popular over the last years  
47 (Chang and Chung 2012; Detert and Weitbrecht 2012; Graham et al. 2010; Strom et al. 2010)  
48 and allow in-situ recording of GSD characteristics. However, overlapping and buried particles  
49 make the use of automated techniques, utilizing photographs, challenging.

50 The complex arrangements of the particles on the river-bed, such as varied orientations,  
51 packing and protrusions also highlight the limitations of using GSD characteristics as a  
52 parameter in bedload transport and flow resistance equations. Even the use of a full GSD is  
53 not sufficient to fully represent the surface morphology and its effect on the flow field (Nikora  
54 et al. 1998; Robert 1988; Robert 1990).

55 Alternatively, the river-bed surface can be considered as a random field of surface elevations  
56  $z(x, y, t)$ , where  $z$  is the surface height at coordinates  $x$  and  $y$  at time  $t$ . Thus, the bed can be  
57 represented as a Digital Elevation Model (DEM). Recent research has shown that high-  
58 resolution DEMs, obtained using various topography measurement technologies, allowed the  
59 use of statistical tools such as Probability Distribution Functions (PDFs) and second-order 2D  
60 structure functions, to understand the structure of water-worked sand-dunes and gravel-beds  
61 and quantify roughness parameters (Aberle et al. 2010; Butler et al. 2001; Friedrich 2010;  
62 Goring et al. 1999; Nikora et al. 1998; Robert and Richards 1988). The hydraulic roughness  
63 can be described as a scale-dependent set of three coefficients, the longitudinal, the  
64 transversal and the vertical roughness, with the vertical roughness represented by the standard  
65 deviation of bed elevation (Aberle and Nikora 2006; Cooper and Tait 2009; Nikora et al.  
66 1998; Smart et al. 2004). Appropriate measurement technologies are needed to obtain the  
67 random field of bed elevations,  $z(x, y, t)$ , and thus being able to define the various inherent  
68 scales of gravel-bed roughness. More attention has to be given to evaluate the measurement  
69 techniques that enable such detailed roughness characterization.

## 70 **Topography measurement techniques**

71 Mainly, three types of remote sensing techniques have been used over the years to obtain  
72 DEMs of gravel beds: bed-profilers, laser-scanners and stereo-photogrammetry. Coleman's  
73 (1997) laboratory experiments with an acoustic bed-profiler proved that this instrument can be  
74 successfully employed to measure submerged topography in a large range of situations. Water  
75 depths ranging from 5-mm to 1000-mm were employed, as well as various downstream and  
76 transverse sampling distances and adjustable acoustic frequency for different vertical  
77 accuracies. The acoustic bed-profiler comprises a sounding probe, which generates ultrasonic  
78 waves that reflect off the sediment bed and are received by the probe. The time of passage of  
79 sound waves is measured electronically and allows determining the distance of the sediment  
80 bed from the probe. Unlike infrared bed-profilers, as in Robert (1988), acoustic bed-profilers  
81 allow submerged topography measurement. Flowing water can be employed in some  
82 situations, and measurements are theoretically unaffected by suspended sediment of size of  
83 the order of the sound wavelength or smaller. Acoustic bed-profilers enable higher spatial  
84 resolution than the generally used 10-mm sampling distance with physical profilers (de Jong  
85 1995; Nikora et al. 1998; Smart et al. 2004). However, regardless of the type of bed-profiler, a  
86 significant amount of time is required to obtain fine-scale DEMs over a larger area.

87 A very high horizontal resolution and vertical accuracy can be achieved by using time-of-  
88 flight Terrestrial Laser-Scanners (TLSs), also called ground-based LiDAR (light detection and  
89 ranging) systems. These scanners find the distance of an object by measuring the round-trip  
90 time of a pulse of laser light. Aberle and Nikora (2006), Cooper and Tait (2009) and Goring et  
91 al. (1999) conducted bed-elevation measurements in drained laboratory flumes using TLSs.  
92 Manufacturer specified vertical accuracies vary from 0.5- $\mu\text{m}$  to 0.1-mm. Heritage and  
93 Hetherington (2007), Hodge et al. (2009) and Smart et al. (2004) conducted surveys with

94 TLSs over exposed gravel bars in natural streams. Laser-scanning is the most precise wide-  
95 range topography measurement device at the moment. However, TLSs' data requires  
96 significant post-processing in the form of filtering to remove systematic errors (Hodge et al.  
97 2008). Also, despite the existence of a multitude of laser-scanners, the cost remains high.  
98 There is another disadvantage, as some of the TLSs cannot be used for measuring submerged  
99 topographies, because of an infrared light pulse absorbed by water (Hodge et al. 2008; Smart  
100 et al. 2004).

101 Similarly to human vision, stereo-photogrammetry makes use of two overlapping 2D images  
102 to obtain one depth image within the Common Field of View (CFoV) of the two images.  
103 Nowadays, commercially available software packages, such as OrthoMAX from Erdas  
104 Imagine®, allow high-resolution DEM recording with digital stereo-photogrammetry, from  
105 either digital images or digitized film photographs. Those packages are often expensive and  
106 limited for specific use. Using OrthoMAX, laboratory-based experiments were carried out by  
107 Butler et al. (2001), Brasington and Smart (2003) and Chandler et al. (2001). DEMs of  
108 exposed, simulated beds, were plotted onto an adjustable grid, with a sampling distance as  
109 small as 1.5-mm. Using ground control points coordinates, Brasington and Smart (2003) and  
110 Chandler et al. (2001) assessed surface precision, with standard errors in vertical  
111 measurement of 2-mm and 1.1-mm, respectively. Stereo-photogrammetry has the advantage  
112 to be relatively easy to set up in both laboratory and field environments, with very quick data  
113 acquisition, yet it generally requires special calibration. Field-based applications were carried  
114 out by Butler et al. (1998) and Carbonneau et al. (2003), to measure the topography of  
115 exposed gravel bars. In addition, Butler et al. (2002) and Westaway et al. (2000; 2001),  
116 proved that stereo-photogrammetry can handle through-water measurement, but a rigorous  
117 strategy must be employed to assess the quality of the DEMs. Whilst stereo-photogrammetry  
118 is to date certainly the most promising technique to remotely sense the dynamic behavior of

119 gravel-beds at the grain scale, the operational process to obtain DEMs is complex. This  
120 generally requires the development of a unique methodology to carefully assess the reliability  
121 of the measurements (Butler et al. 1998). Another disadvantage is oblique scanning from two  
122 different viewpoints, which causes shadowing behind protruding particles and results in  
123 erroneous data in those affected areas.

## 124 **Objective**

125 Often laboratories have access to one measurement technique for gravel-bed data acquisition.  
126 The study's objective is to compare bed-roughness data collected with the above described,  
127 most commonly used, three measurement methodologies, which were available for this  
128 project. The study is split in two parts, which build upon each other. Initially, a screeded bed  
129 was water-worked and once fully developed, the bed was measured with all three available  
130 measurement techniques, namely acoustic bed-profiler, laser scanner and stereo-  
131 photogrammetry. The water-worked data are used to study the suitability of the DEMs to  
132 undertake statistical analysis of the bed roughness and assess the differences in quantitative  
133 and qualitative roughness characteristics for the same roughness area, but different  
134 measurement methodology. The analysis focuses on the hydraulic roughness, represented by  
135 the standard deviation of bed elevations, and bed-elevation Probability Distribution Functions  
136 (PDFs) and second-order structure functions (semivariograms) of the DEMs. In order to  
137 compare the water-worked roughness characteristics, screeded bed topography, recorded with  
138 the acoustic bed-profiler, is assessed.

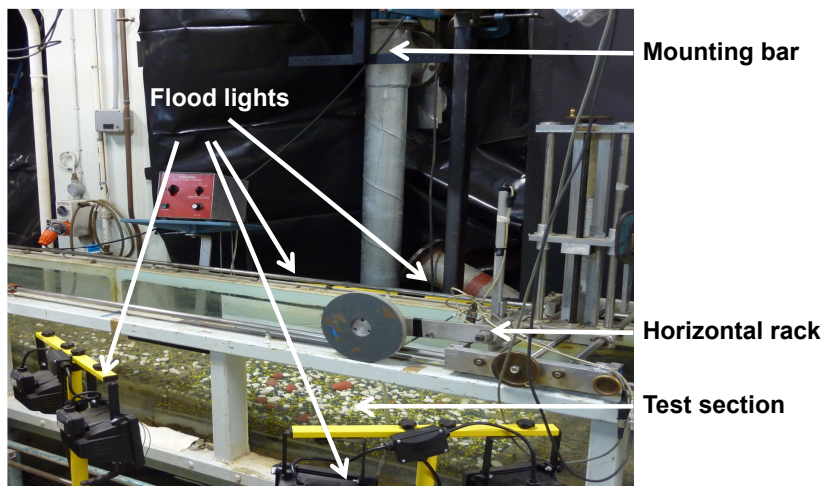
139 The second part of the study presents the methodological improvements that were made for  
140 the stereo-photogrammetric setup, and how those improvements affect the quality of recorded  
141 DEMs.

## 142 DATA COLLECTION

### 143 The experimental setup

144 Data collection was undertaken in the Fluid Mechanics Laboratory of The University of  
145 Auckland, using a 19-m long sediment-starved tilting flume, with 0.45-m width and 0.5-m  
146 depth. For the presented experiments, the slope of the flume bed was set to 0.45.  
147 Measurements were obtained on a vertically adjustable test section, located 10-m downstream  
148 of the flume inlet, comprising of a fixed bed with a 950-mm long and 450-mm wide recess.  
149 The recess was filled with graded, rounded and colored gravel (each class of sediment, except  
150 the smallest one was painted with a different color, using white, yellow, green, blue and red).  
151 The use of painted gravel particles was necessary for a parallel study on cluster formation and  
152 sediment tracking. The sediment had a median size of the intermediate particle axis  $D_{50} = 7$ -  
153 mm, a minimum sediment size of 0.7-mm, a maximum gravel size of 50-mm and a geometric  
154 standard deviation of the grain distribution, calculated as  $\sqrt{D_{84}/D_{16}}$ , of 2.98. To enable  
155 topography measurement, the test section was equipped with a horizontal rack for the acoustic  
156 bed-profiler, as well as an overhead mounting bar for stereo-photogrammetry equipment, on  
157 which two cameras were mounted (Figure 1). The initial screeded bed was created by placing  
158 randomly mixed sediment into the base of the vertically adjustable survey area and the surface  
159 was flattened to a thickness of 100-mm, parallel to the flume bed. The topography of the  
160 initial manually screeded bed was measured with the acoustic bed-profiler. The gravel-bed  
161 was then water-worked and naturally armored over four hours, at a constant flow rate  $Q = 66$ -  
162 L/s, monitored by a pre-calibrated pressure gauge. The water depth was kept constant at 200-  
163 mm, and adjusted using a sharp-edged weir at the downstream end of the flume. A steady  
164 uniform flow was maintained throughout the experiment with a Froude number  $Fr = 0.58$ .

165 The area used for direct comparison of the three measurement techniques was 0.35-m long  
166 and 0.3-m wide (Figure 2). As the laser-scanner could not be used directly at the flume, a  
167 metallic tray was submerged into the initially screeded mixture, completely covered by the  
168 sediment layer, allowing the careful transportation of the 0.35-m long and 0.3-m wide water-  
169 worked gravel-bed sample to the location, where the laser is housed. Whilst water-working,  
170 the upper sediment layer eroded downstream. The experiment was stopped just when the tray  
171 started to be exposed. Thereafter, the bed topography was measured with the acoustic bed-  
172 profiler. The flume was then drained to allow in-air stereo-photogrammetry measurement.  
173 Finally, the metallic tray was carefully uncovered and moved to the location of the laser-  
174 scanner, to undertake the laser-scanner data collection.



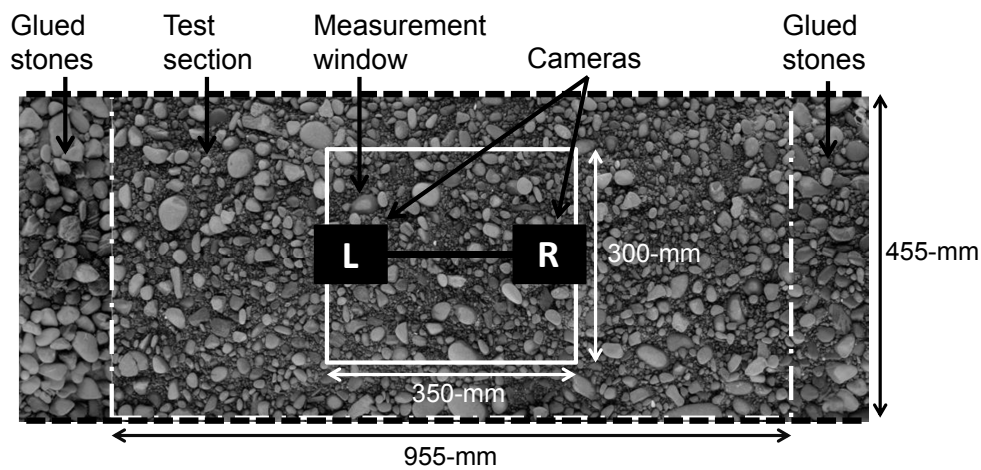
175

176 **Fig. 1.** Flume setup

### 177 **Acoustic bed-profiler**

178 Measurements of the submerged gravel-beds, at initial screeded and final water-worked  
179 stages, were undertaken with a reduced flow rate to avoid suspended sediment that could lead  
180 to erroneous data. The acoustic bed-profiler is comprised of a sounding probe, located 100-  
181 mm above the sediment bed, mounted on a rack above the flume, traversing the measurement

182 section in flow direction, and an optical potentiometer of 256 increments per revolution,  
183 attached to the hub of a 200-mm diameter wheel, tracking the probe location in the  
184 downstream direction. With a sound wave of frequency  $f = 2$ -MHz it provided a theoretical  
185 vertical accuracy of 0.37-mm (see Table 1). 2D longitudinal bed-elevation profiles were  
186 acquired and subsequently DEMs were obtained with a sampling distance of 2.45-mm  
187 downstream (based on the number of increments on the potentiometer and wheel size) and  
188 2.54-mm transverse (0.1-inch on the scale utilized), representing the physical grid over which  
189 the measurements were done.



190

191 **Fig. 2.** Gravel bed and measurement window

## 192 **Laser-scanner**

193 The topography of the final water-worked bed, restricted to the area bounded by the edges of  
194 the metallic tray, was measured with an Inition MVT CLS60 hand-held laser-scanner,  
195 available in The University of Auckland Automated Systems Laboratory. Because of the short  
196 arm of the laser, it could not be used directly above the flume and required the transportation  
197 of the gravel-bed sample. Once transported, the sample was scanned vertically from a distance  
198 of 100-mm by making several overlapping stripes. The theoretical vertical accuracy is  
199 quantified as 0.05-mm (manufacturer specified), and data is recorded on a non-uniform spatial

200 grid. The merging of the overlapping stripes was operated automatically by the instrument's  
201 software, with the process repeated until successful merging was obtained. The laser-scanner  
202 has the advantage that both depth and color information are recorded, although color  
203 information was not used for this study. Finally, data was saved as an ASCII file and was  
204 directly read into MATLAB®. The non-uniform data cloud was transformed to a uniform grid  
205 with 1.45-mm sampling distance (Table 1). Measurements took place in non-submerged  
206 conditions. However, preliminary tests showed that wet conditions, e.g. with wet particle  
207 surfaces, have no detrimental effect on the laser's accuracy (see Table 2).

## 208 **Stereo-photogrammetry**

209 Stereo-photogrammetric measurements of the exposed water-worked bed were carried out  
210 with two Nikon D90 digital consumer cameras, with an 18-mm lens and a 5.5- $\mu\text{m}$  pixel pitch  
211 (12.3-megapixels). The two cameras were attached on a frame 1-m above the flume,  
212 mechanically aligned with a 280-mm baseline between the cameras, using a mounting bar.  
213 The settings for both cameras were manually adjusted to be identical (shutter speed of 1/3-s,  
214 F/22 aperture, ISO 200) and manually focused on the gravel-bed. The Common Field of View  
215 (CFoV) of the two cameras, chosen to be larger than the test section, defined the area over  
216 which depth information was extracted. Initially, stereo images of the calibration  
217 checkerboard were taken in various positions inside the hydraulic flume, covering all degrees  
218 of freedom and most of the cameras' CFoV (Zhang 1998). Using MATLAB® and Bouguet  
219 and Perona's (1998) camera calibration toolbox, the intrinsic parameters of the two cameras  
220 (focal length, principal point, skew among others), and the extrinsic parameters of the stereo  
221 setup (translation and rotation between the two cameras) were determined. Radial and  
222 tangential lens distortion of the two cameras was modeled using a 6<sup>th</sup> order polynomial. The  
223 calibration data enabled the photographs of the gravel-bed to be rectified to epipolar

224 geometry, where corresponding points between the left and right images are on the same scan  
225 lines, after distortion is removed. From the rectified images of the gravel-bed and the  
226 calculated disparity search range, the Symmetric Dynamic Programming Stereo-  
227 photogrammetry (SDPS) algorithm allowed getting a map of the bed surface elevations, also  
228 called disparity map, within the CFoV (Gimel'farb 2002). A point cloud is extracted, with  
229 sampling distance between measured data points representing the pixel size on the gravel-bed  
230 images as taken with the Nikon D90s from a distance of 1-m. Finally, the data were  
231 transferred to a uniform grid with a sampling distance of 1-mm (Table 1). The best vertical  
232 accuracy achievable by the setup in these conditions was calculated as 1-mm.

### 233 **Improved stereo-photogrammetric setup**

234 The results obtained with stereo-photogrammetry in the first part of the study were not  
235 satisfactory, as shown in the 'Results' section. Thus, work was done to obtain better DEMs  
236 using photogrammetric means.

237 The following improvements were made, which can be used as a checklist to obtain high-  
238 quality DEMs. Firstly, the measurement section needs to be illuminated as evenly and as best  
239 as possible. In addition to placing light sources strategically, any reflection bouncing off the  
240 measured object can negatively influence the measurement process. Thus, as a first step, the  
241 light sources outside the flume were changed from initially four flood lights to two 1-m long  
242 neon lights, which were placed behind a dissipative sheet, resulting in a homogeneous  
243 illumination of the measurement area. Secondly, the painted gravels were replaced by natural  
244 gravel particles, eliminating any reflection bouncing off the gravel-bed. The third change was  
245 to resize the CFoV, by reducing the distance from the cameras to the gravel bed. This change  
246 is not responsible in its own for the reduction of streaks and noise in the DEMs, but it led to  
247 an enhanced vertical accuracy of 0.34-mm (see Table 1). In addition, the measurement

248 resolution increased to approximately 30.8-million points/m<sup>2</sup>, equivalent to 0.18-mm pixel  
249 size on the gravel-bed surface. Fourthly, a modified checkerboard was used. The  
250 checkerboard used previously was made of plastic, and was a cause of light reflection. It did  
251 not always allow correct corner recognition during the calibration process leading to  
252 inaccurate calibration parameters. Finally, the frame mounting bar holding the cameras was  
253 adjusted to allow a faster and more accurate calibration process. The cameras' mounting bar  
254 could be rotated at 90°, allowing photographs of the checkerboard to be taken with the  
255 checkerboard mounted on a tripod outside the flume.

256 A simple MATLAB® program was developed to evaluate the accuracy of the calibration step,  
257 based on the reprojection error. Using the calibration results (summarized in the projection  
258 matrices of the two cameras), the estimated corners of the checkerboard, originally in 3D  
259 world coordinates, can be reprojected onto the 2D calibration images. The estimated corners  
260 are compared with the actual corners detected with the subpixel corner detection algorithm  
261 available with MATLAB®. The reprojection error, in pixel, is defined as the difference  
262 between the actual corners and the estimated corners. A decrease in reprojection error shows  
263 that the calibration parameters (both intrinsic and extrinsic) are better estimated. In the  
264 absence of an external assessment of DEMs quality, an internal assessment of the calibration  
265 step was undertaken to contrast two DEMs obtained with stereo-photogrammetry.

## 266 **Data post-processing**

267 The same data post-processing procedure was applied to all DEMs obtained in the first part of  
268 the study. The DEM obtained with the improved stereo-photogrammetric setup (Figure 5),  
269 forming the second part of the study, was of high quality, with no spikes observed and the  
270 following data post-processing procedure was not needed. Data post-processing consisted of  
271 removing measurement spikes and interpolating gaps. Spikes, which were outside the

272 minimum/ maximum bed elevations, as found with the acoustic bed-profiler  $DEM \pm 2\text{-mm}$ ,  
273 were removed. Minor spikes, due to measurement imprecision and noise, were automatically  
274 detected as data points lying outside their four neighbors' elevation, allowing for a  $\pm 3\text{-mm}$   
275 threshold. The threshold of 3-mm is specific to the used sediment mixture and was obtained  
276 through manual testing. The gaps generated by the removal of spikes were automatically  
277 filled by the average elevation of the four neighboring data points.

278 Before analyzing the DEMs statistically, a detrending algorithm was applied on each DEM.  
279 Surface detrending aims to remove larger scale trends than the grain-scale, such as bed slopes,  
280 which could obscure DEMs properties and bias grain roughness statistics. This also removes  
281 any deviation of the measurement instruments from a parallel positioning to the sediment bed.  
282 In accordance with Andreas and Trevino (1997), and Goring et al. (1999), a second-order  
283 biquadratic removing filter was applied, as this reduced the variance of the original data series  
284 the most. The difference in variance between the original and the detrended signals was  
285 significant, and exceeded the square of the measurement resolutions. Finally, all DEMs were  
286 normalized to have a mean bed elevation equal to zero, and rotated in order to align the DEMs  
287 with the flow direction.

## 288 **STATISTICAL ROUGHNESS ANALYSIS**

289 Statistical roughness analysis serves as the basis for the comparison of the employed  
290 measurement techniques and whether the obtained DEMs (Figure 4) warrant to be used for  
291 future studies on gravel-bed roughness characterization. Initially, Probability Distribution  
292 Functions (PDFs) were obtained, representing the distribution of surface elevations.  
293 Parameters like skewness, kurtosis and standard deviation of surface elevations were  
294 extracted from the detrended surfaces. Similar to previous work by Aberle and Nikora (2006),

295 Cooper and Tait (2009) and Nikora et al. (1998), the vertical roughness height was estimated  
 296 using the standard deviation of the bed elevation  $\sigma_z$ .

297 In addition, generalized second-order 2D structure functions were used, defined by Nikora et  
 298 al. (1998) in discrete form as:

$$299 \quad D_{G2}(\Delta x, \Delta y) = \frac{1}{(N-n)(M-m)} \sum_{i=0}^{N-n} \sum_{j=0}^{M-m} \{|z(x_i + n\delta x, y_j + m\delta y) - z(x_i, y_j)|\}^2 \quad (1)$$

301 where,  $\Delta x = n\delta x$  and  $\Delta y = m\delta y$ ;  $\delta x$  and  $\delta y$  are sampling intervals in the longitudinal and  
 302 transverse directions respectively;  $n=1,2,3,\dots,N$  and  $m=1,2,3,\dots,M$ .  $N$  and  $M$  are the number of  
 303 samples in the same two directions. The relationship in Eq.1 is used to represent the  
 304 generalized 1D second-order structure functions, as well as isopleth maps (contour plots) of  
 305 the 2D structure functions. To enable a direct comparison between the various measurement  
 306 techniques, the structure functions were normalized with the 'saturation level'  $2\sigma_z^2$  and the  
 307 contours of  $D_{G2}$  were plotted as proportions of the saturation level.

308 The irregular nature of gravel-bed profiles suits the use of generalized structure functions to  
 309 investigate the fractal properties of the bed surface, which provides information about the  
 310 inherent scales of roughness present on the gravel-bed surface. A structure function has three  
 311 regions: a scaling region with uniform slope at small lags, a saturation region at large lags,  
 312 where the slope is zero, with a transition region in between, where the slope decreases (Butler  
 313 et al. 2001; Goring et al. 1999; Nikora et al. 1998; Robert and Richards 1988).

314 At small spatial lags, the scaling region can be fitted by a power function of the form  
 315  $D(\Delta x) \propto \Delta x^{2H_x}$  (Figure 7a) and  $D(\Delta y) \propto \Delta y^{2H_y}$  (Figure 7b). Butler et al. (2001) and Robert  
 316 (1988) showed that when plotted in log-log scale, the use of a power function allows the  
 317 determination of the directional Hurst exponents  $H_x$  and  $H_y$ , representing a basic method to

318 estimate the fractal dimension of series of data along the downstream and transverse  
319 directions, respectively. They also showed that the directional fractal dimensions of series of  
320 points, also called Hausdorff dimensions, can be estimated from the slopes of the linear parts  
321 of the structure function, using the relation  $2 - H$  and can be linked to different roughness  
322 scales.

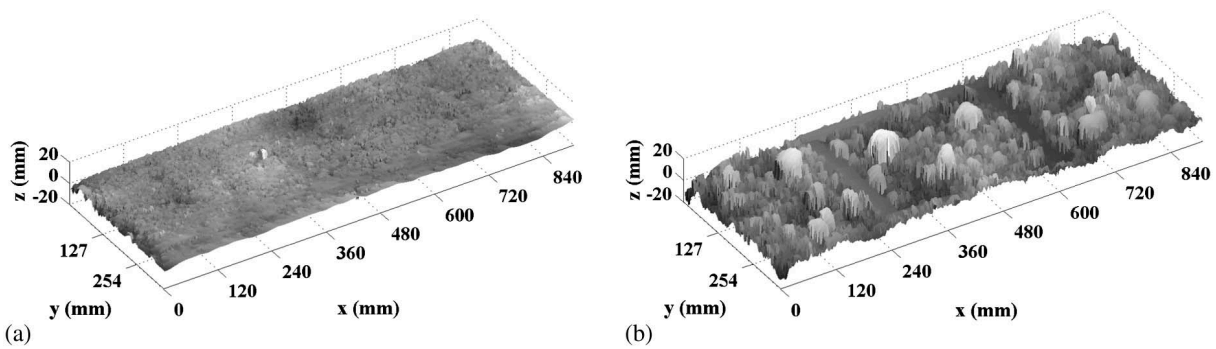
## 323 **RESULTS**

### 324 **Digital Elevation Models (DEMs)**

325 Both, the initial screeded and final water-worked beds, were measured with the acoustic bed-  
326 profiler over the complete recess section (Figure 3). The manually screeded bed (Figure 3a) is  
327 composed of grains of different sizes with buried bigger particles. The surface is flat and  
328 uniform, with bed elevations between -12.3-mm and 7.2-mm, and sediment randomly  
329 distributed. In contrast, the water-worked bed (Figure 3b) presents a heterogeneous surface,  
330 with a larger range of bed elevations, of -24.4-mm to 29.7-mm. The surface, composed of  
331 coarse grains, with small particles filling the holes between them, presents the evidence of  
332 armoring. In Figure 3b, the edges of the metallic tray are clearly visible, defining the region  
333 over which the statistical analyses were conducted.

334 The DEMs of the water-worked bed vary notably (Figure 4). With the acoustic bed-profiler,  
335 the surface appears smooth with little noise (Figure 4a). Any visible errors are concentrated  
336 on the particles' edges, where major elevation changes occur rapidly. The laser-scanner's  
337 DEMs (Figure 4b) are similar to those obtained with the acoustic bed-profiler. Although,  
338 theoretically, the higher resolution of the laser scanner should enable the edges of the particles  
339 to be more representative, this is not observed, due to measurement noise. The DEM obtained  
340 with stereo-photogrammetry (Figure 4c) is of least quality, despite the highest resolution. Not

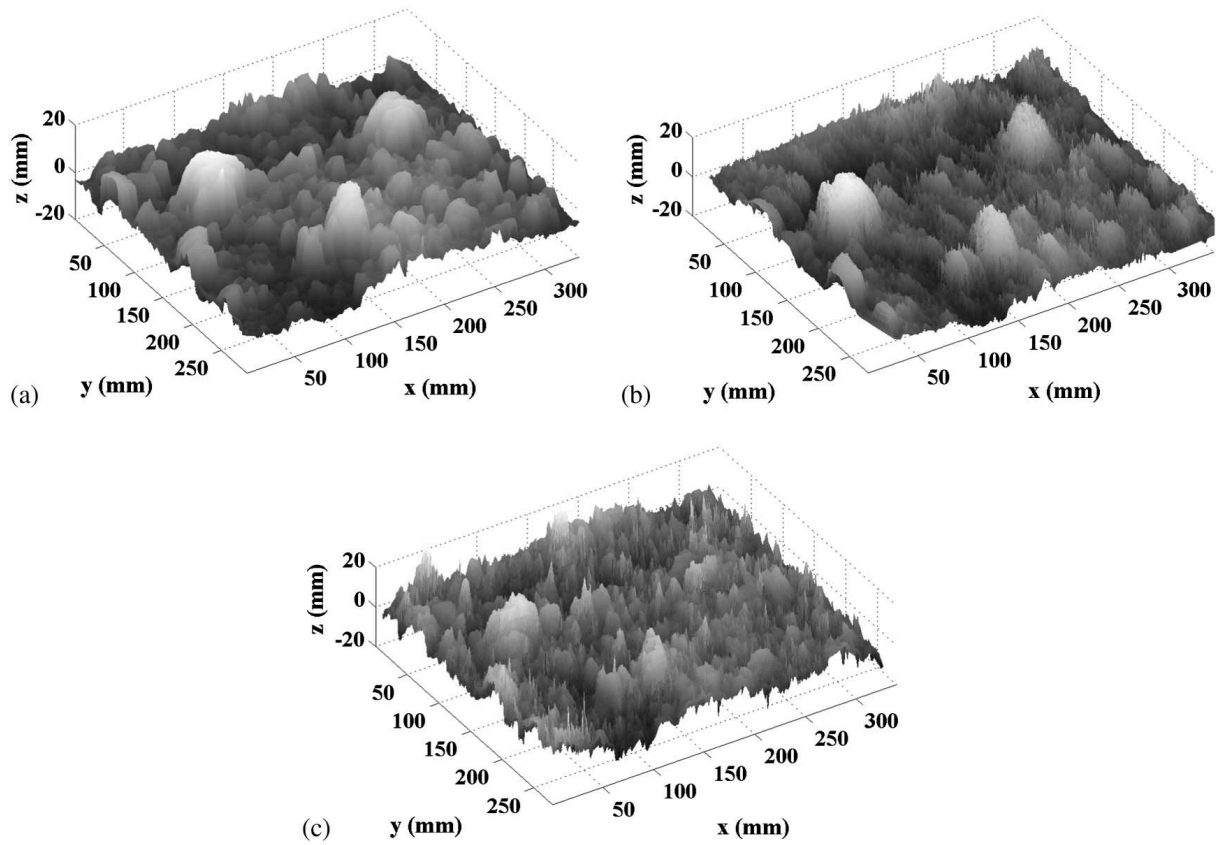
341 all of the major gravel particles are well captured. Detailed inspections also show major noise,  
342 even after despiking, thus prompting us to investigate the cause of the noise further, which  
343 resulted in the methodological changes made on the photogrammetric setup presented in  
344 section ‘Improved stereo-photogrammetric setup’. The changes led to a decreased  
345 reprojection error. The obtained DEM presented in Figure 5 used calibration results with a  
346 standard deviation in reprojection error of 0.2-pixels, compared to the reprojection error for  
347 the DEM of Figure 4c with a standard deviation of 1.15-pixels. The measurement noise is  
348 correctly suppressed by an improved photogrammetric process, and all particles on the gravel-  
349 bed surface are correctly represented. Consequently, the decreased reprojection error results in  
350 a visually appealing DEM (Figure 5), plotted on a very fine grid, with 0.2-mm sampling  
351 distance.



353 **Fig. 3.** Detrended DEMs obtained with the acoustic bed profiler in submerged conditions,  
354 after despiking, for (a) the initial screeded bed; (b) the final water-worked bed

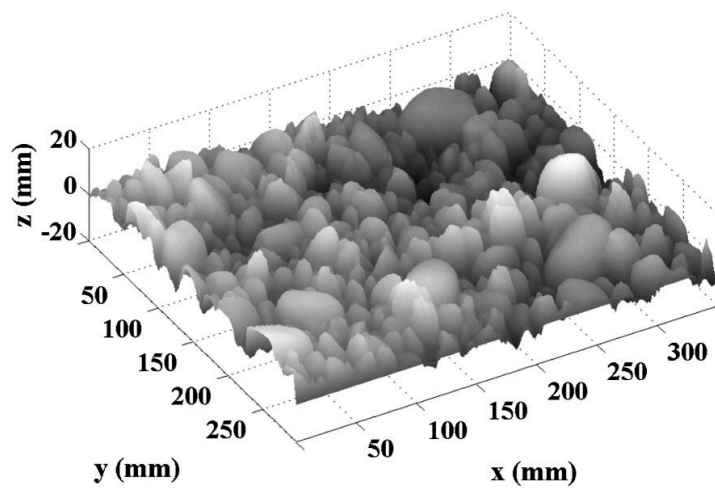
### 355 **Probability Distribution Functions (PDFs)**

356 PDFs were generated to allow a statistical comparison of texture parameters for the various  
357 measurement techniques, such as skewness, kurtosis, range of elevations, and the vertical  
358 roughness length. In addition, it is a useful tool for comparing initial screeded and final water-  
359 worked beds and studying the influence of armoring.



360

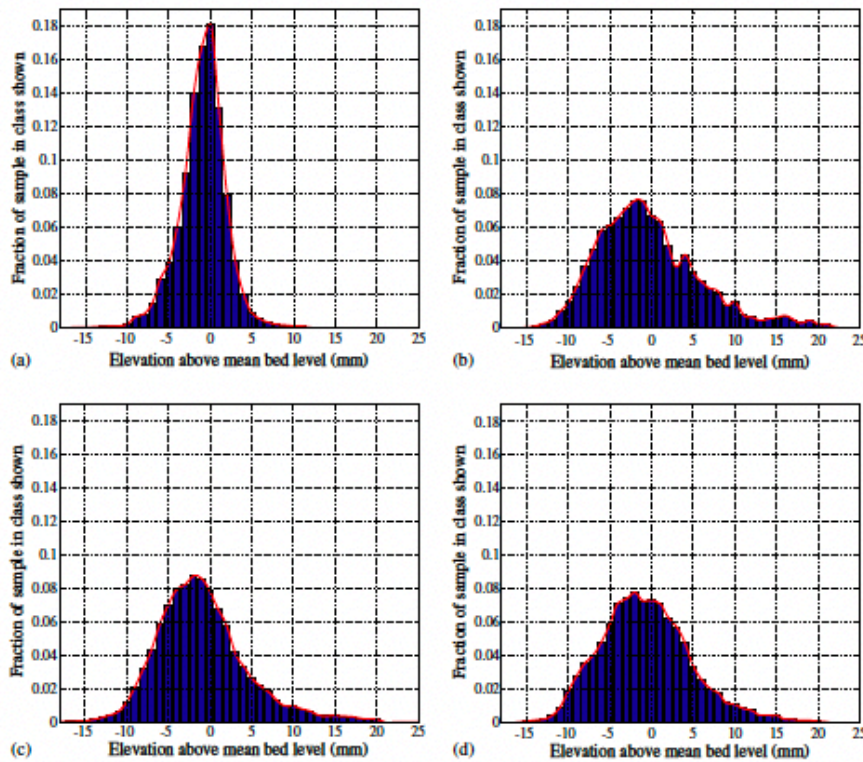
361 **Fig. 4.** Detrended DEMs of the water-worked bed, after despiking, focused on the region  
 362 within the metallic tray, obtained with (a) the acoustic bed profiler; (b) the laser scanner (dry  
 363 condition); (c) stereophotogrammetry



364

365 **Fig. 5.** DEM of a water-worked bed obtained with the improved stereophotogrammetric setup

366 In accordance with previous studies, e.g. Aberle and Nikora (2006) and Cooper and Tait  
 367 (2009), the initial screeded bed is negatively skewed (Figure 6a), whereas the water-worked  
 368 beds are positively skewed (Figures 6b-c-d), for all three measurement techniques. The PDFs  
 369 of Figure 6 also visualize the augmentation of geometrical roughness during the armor layer  
 370 development, i.e. the augmentation of particles of higher elevations with respect to the mean  
 371 bed level, which protrude into the flow. A larger range of bed elevations is observed for a  
 372 water-worked bed (Figures 6b-c-d), compared with the narrower range for a screeded bed  
 373 (Figure 6a). As Table 2 shows, after water-working the initially screeded gravel-bed, the  
 374 skewness coefficient and the standard deviation of the bed elevation,  $\sigma_z$ , increase, and  
 375 characterize the coarsening of the gravel-bed surface. No significant change in the kurtosis  
 376 value was observed.



377  
 378 **Fig. 6.** PDFs obtained with (a) the acoustic bed profiler over the screeded bed, and over the  
 379 restricted water-worked bed with (b) the acoustic bed profiler; (c) the laser scanner (dry  
 380 condition); (d) stereophotogrammetry

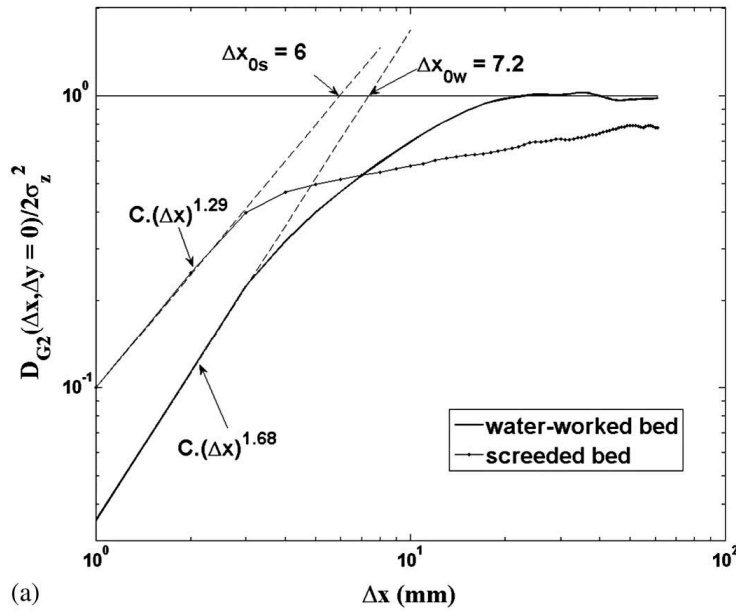
381 For laser-scanner DEMs, similar statistics for the dry and wet surfaces are obtained, indicating  
382 a good reproducibility of the results. Although, statistically, the DEM obtained with the initial  
383 stereo-photogrammetric setup, results in a reduced skewness and roughness length, the  
384 statistics do not vary to the extent, as the visible DEM shortcomings would suggest. The  
385 statistics of the DEM obtained with the improved stereo-photogrammetric setup, as obtained  
386 in the second part of the study, are not presented, as the studied water-worked gravel-bed is  
387 different. Figures 6b-c-d show that the range of bed elevations is similar for all three DEMs,  
388 but the distribution of bed elevations in the different ranges varies. The DEM obtained with  
389 the acoustic bed-profiler presents the lowest sorting in bed elevations, with the smallest  
390 fraction of bed elevations around the zero mean-bed level. Noise present in the DEMs  
391 obtained with the laser-scanner and the initial stereo-photogrammetric setup causes more  
392 particles to be distributed around the zero-mean and less particles at low and high elevations.

### 393 **Second-order structure functions**

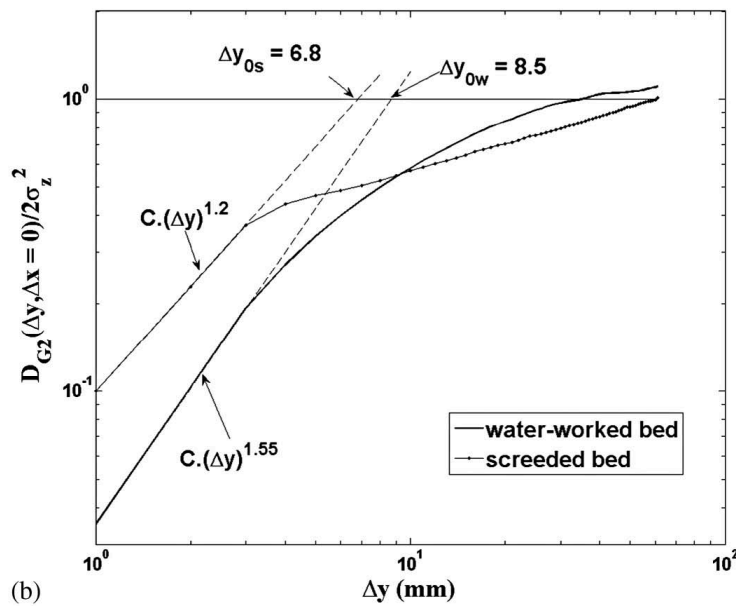
394 Previous research showed that the value of the Hurst exponent is inversely proportional to the  
395 degree of complexity of the gravel-bed surface (Aberle and Nikora 2006; Cooper and Tait  
396 2009; Nikora et al. 1998). For our study, the screeded bed has a smaller Hurst exponent than  
397 the water-worked bed, which suggests that the screeded bed surface, with numerous smaller  
398 bed elevations, is more complex than the water-worked bed, which comprises a larger range  
399 of bed elevations (Figure 7). This correlates well with previous experiments of Aberle and  
400 Nikora (2006), where Hurst exponents of the man-made screeded beds are smaller than those  
401 of water-worked beds, with Hurst exponents increasing with increasing discharge.

402 The scaling region of the structure function provides information about the horizontal  
403 roughness indices, which can be determined from the slope breakpoint, located at the  
404 intersection between the tangent to the scaling region slope and the saturation level

405 asymptote, in both x and y direction. The horizontal roughness indices ( $\Delta x_0$  and  $\Delta y_0$ ) are larger  
 406 for water-worked beds, than for screeded beds (Figure 7). The sediment particles on the bed  
 407 surface coarsen during water-work.



(a)

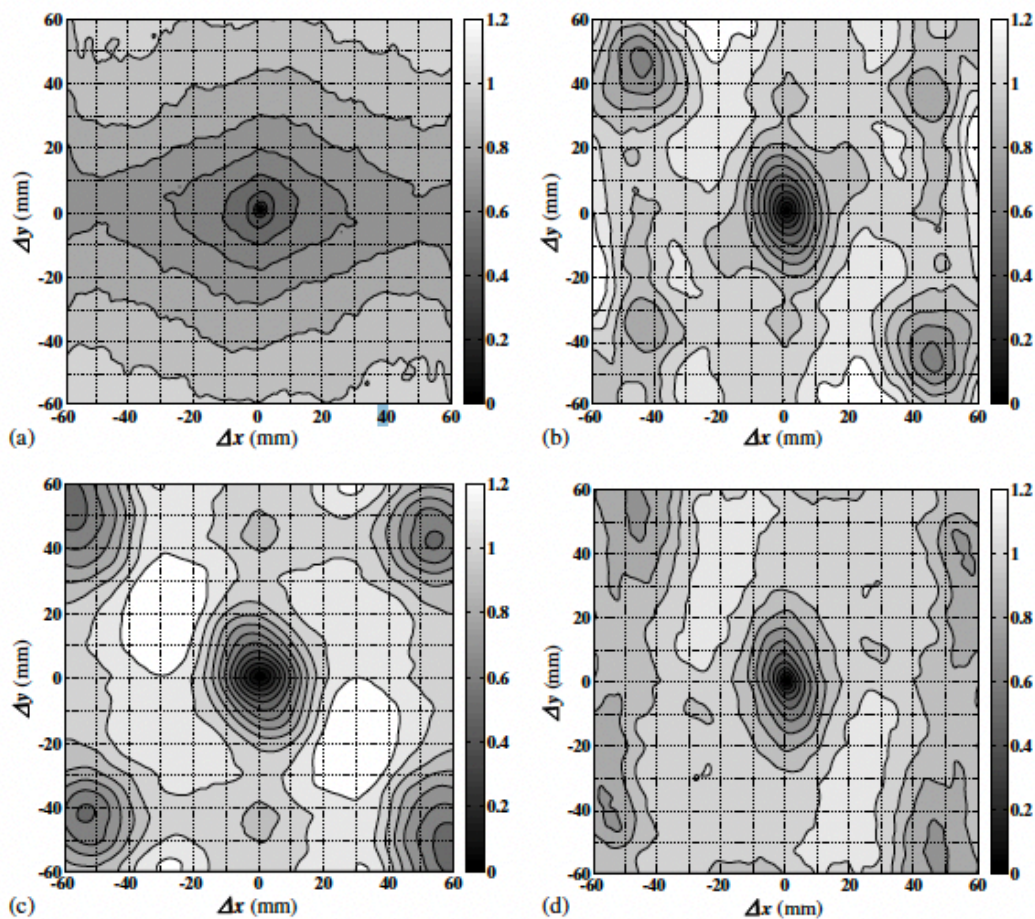


408 (b)

409 **Fig. 7.** Generalized second-order structure functions plot in a log-log scale, for (a)  $\Delta y = 0$ ; (b)  
 410  $\Delta x = 0$

411 As presented by Aberle and Nikora (2006) and Friedrich (2010), the use of isopleth maps of  
 412 2D structure functions provides useful information on the surface forming mechanisms during

413 the armor layer development. Contour lines at small spatial lags are circular for the screeded  
414 bed (Figure 8a), indicating isotropy of the surface structure and a random organization,  
415 whereas the contour lines of all water-worked beds are characterized at small spatial lags by  
416 an elliptical shape (Figure 8b-c-d). This finding agrees with previous work by Aberle and  
417 Nikora (2006), Cooper and Tait (2009) and Goring et al. (1999). Geometrically, the elliptical  
418 shape of the contour lines reflects the general elliptical form of the dominant particles and an  
419 anisotropic surface structure of the bed. In this study, particles rotate to align their long axis  
420 across the flow direction (Figure 8b-c-d), as observed also by Goring et al. (1999).



421  
422 **Fig. 8.** Contour lines of structure functions obtained with (a) the acoustic bed profiler over the  
423 screeded bed, and over the restricted water-worked bed with (b) the acoustic bed profiler; (c)  
424 the laser scanner (dry condition); (d) stereophotogrammetry

## 425 **DISCUSSION**

426 The three measurement technologies employed in this study, theoretically allow grain-scale  
427 elevation measurements of water-worked beds in a laboratory flume. In their work, Lane et al.  
428 (1994) estimated that between 4,000 and 10,000-points/m<sup>2</sup> (equivalent to 10-mm to 16-mm  
429 sampling distance) are necessary to survey the morphology of a braided proglacial stream at  
430 the grain scale. In the first part of our laboratory study, utilizing sediment with  $D_{50} = 7$ -mm,  
431 DEMs with resolutions between 160,000 and 1,000,000-points/m<sup>2</sup> (equivalent to 1-mm to  
432 2.54-mm sampling distance) were obtained. For the 0.35-m long and 0.3-m wide  
433 measurement window, this equates to approximately 16,870 data points for DEMs obtained  
434 with the acoustic bed-profiler. DEMs with around 49,940 and 105,000 data points were  
435 obtained for the laser-scanner and initial stereo-photogrammetric setup, respectively. Our  
436 statistical analysis showed that the measurement resolution is not the only key parameter  
437 when comparing the quality of the DEMs. The initial stereo-photogrammetric setup had the  
438 highest measurement resolution, with statistics showing only a minor deviation from the other  
439 DEMs, but visual observation of the DEM showed substantial shortcomings (Figure 4c).  
440 Problems were encountered with the reflection of the painted gravel particles, causing  
441 inaccuracies in creating the map of the bed surface elevations, and thus resulting in spikes in  
442 the DEM. Compared to the other two measurement techniques, stereo-photogrammetry  
443 requires a multi-stage recording process (calibration of cameras, creating depth map,  
444 extracting point cloud), with errors of various stages accumulating. Calibration inaccuracies  
445 for the initial stereo-photogrammetric DEM (Figure 4c), prevented the correct rectification of  
446 the gravel-bed stereo pairs to epipolar geometry. With stereo-photogrammetry, the recording  
447 time was the quickest of all techniques once the cameras were calibrated, which required 30-  
448 minutes (to obtain photographs of the checkerboard and extract the calibration parameters in  
449 MATLAB®). Calibration results could then be utilized to rectify all images of the gravel-bed

450 acquired with the same setup, i.e. when no changes were made on the cameras parameters or  
451 the setup geometry.

452 The laser-scanner is theoretically the most accurate measurement instrument for this study,  
453 with a theoretical vertical accuracy of 0.05-mm. Laser scanning enabled a fast survey of the  
454 measurement window. However, the size of the latter was restricted by the laser arm. It also  
455 required the transportation of the gravel sample to the location of the laser, and required  
456 merging of scanned areas, as it was not able to scan the whole measurement window in one  
457 scan. Spikes were encountered during the merging process, which had to be removed  
458 automatically, but measurement noise remained, reducing the quality of the final DEM.

459 Finally, the acoustic bed-profiler measured the bed elevation with a theoretical vertical  
460 accuracy of 0.37-mm. It was the most straightforward measurement equipment to use and was  
461 the only technique in our study that enabled measurement of the submerged gravel-bed.  
462 During water-working, sediment of sizes larger than 2-mm were transported in suspension,  
463 thus requiring to halt the experiment during measurements, to ensure no suspended sediment  
464 particles were picked up by the recording. The recording time was the longest of the three  
465 studied techniques, which can be a significant drawback when successive DEMs have to be  
466 obtained of evolving processes.

467 Visually, DEMs obtained with the acoustic bed-profiler and the laser-scanner seemed well  
468 suited for statistical roughness analysis, whereas the DEM obtained with the initial stereo-  
469 photogrammetric setup showed an obvious lack of topographical accuracy. Following the  
470 visual study of the DEMs, the DEMs underwent statistical roughness analysis. The vertical  
471 roughness length, as expressed with the standard deviation of bed elevations  $\sigma_z$ , is similar for  
472 all DEMs (see Table 2). It was found  $\sigma_z = 5.36 \pm 0.4$ . As observed visually, the grains'  
473 edges were not represented accurately in the DEM obtained with the acoustic bed-profiler,

474 resulting in flatter gravel tops and thus overestimate the standard deviation of bed elevation.  
475 The laser-scanner allowed a good reproducibility of the results when tested over a dry and wet  
476 gravel-bed surface, as seen in Table 2.

477 Statistical results of the PDFs and generalized second-order structure functions, as presented  
478 in Figures 6, 7 and 8, show a good agreement for the various DEMs. This indicates that  
479 although visible differences in the topography of the DEMs were observed, those  
480 measurement differences are less identifiable when DEMs are described statistically.

481 Our evaluation study highlights that a detailed visual validation of the DEMs is crucial for  
482 gravel-bed studies, as significantly different DEMs of the same topography can produce  
483 similar roughness statistics. Quantitative validation of DEMs quality can only be made  
484 through comparison of obtained bed elevations with a ground truth, which is often practically  
485 not feasible, as in our presented study. In our study, the laser-scanner was theoretically the  
486 most accurate instrument, but noise in the DEM prevented using the laser-scanner data as a  
487 ground truth. Other studies evaluate the error rate of one measurement technique by  
488 comparing several records with each other, like it was done in studies employing stereo-  
489 photogrammetry (Butler et al. 1998; Carbonneau et al. 2003; Chandler et al. 2001).

490 The obtained initial stereo-photogrammetric DEM was of inferior quality (Figure 4c) and  
491 prompted additional testing to obtain high-quality DEMs, as the literature research showed  
492 that low-cost stereo-photogrammetric measurements of gravel-bed topographies will be useful  
493 for future studies. In previous hydraulic applications of stereo-photogrammetry, semi-metric  
494 cameras were used (Butler et al. 1998; Butler et al. 2001; Butler et al. 2002), in addition to  
495 commercial photogrammetric software (Brasington and Smart 2003; Butler et al. 1998;  
496 Carbonneau et al. 2003; Chandler et al. 2001; Rapp et al. 2012; Westaway et al. 2001). The  
497 calibration technique relied on automatic block-bundle adjustment, or self-calibration

498 technique. Targets were required, generally a large number, to be arranged on the surface to  
499 survey. The 3D locations of the targets are determined with Leica total stations, making for  
500 the duplicity of measurement instruments in the experiments and increasing the chance of  
501 errors propagating. In addition, targets glued on the riverbed surface disturb the experiment  
502 and are not complementary with an otherwise remotely sensed topography.

503 In our low-cost stereo-photogrammetric setup, we decide to use Zhang calibration technique  
504 (Zhang 1998), which requires a planar calibration pattern (called checkerboard) to be  
505 photographed in several positions. Although it requires additional time to obtain these images,  
506 this calibration technique avoids using ground control points disposed on the riverbed. It is  
507 also considered that Zhang calibration will be more suitable for field work, where the areal  
508 coverage is larger than inside laboratory flumes, which would mean that more targets are  
509 required, compared to a laboratory study. Using ground control points, measured with total  
510 stations, has however the advantage that it provides information to assess externally the  
511 DEM's quality. With our proposed low-cost stereo-photogrammetric setup, a simple  
512 MATLAB® program was prepared to evaluate the accuracy of the calibration step, which was  
513 identified as a source of error for the DEMs. The evaluation is based on the reprojection error.  
514 Following the checklist provided in section 'Improved stereo-photogrammetric setup' results  
515 in a decreased reprojection error, which in turn enables a high-quality DEM to be obtained  
516 (Figure 5).

517 Besides exhibiting the best accuracy qualitatively, the DEM obtained with the improved  
518 stereo-photogrammetric setup has a sampling distance of 0.2-mm on the gravel-bed surface,  
519 which corresponds to the highest DEM resolution so far obtained for gravel-bed studies,  
520 compared to the previous minimum of 1-mm obtained by Cooper and Tait (2009) with TLS  
521 and by Carbonneau et al. (2003) with stereo-photogrammetry.

## 522 CONCLUSION

523 A laboratory study to evaluate available measurement techniques to study the hydraulic  
524 roughness for gravel beds is presented. The use of an acoustic bed-profiler, a hand-held laser-  
525 scanner and stereo-photogrammetry allowed acquisition of DEMs. Analysis techniques, such  
526 as determination of the vertical roughness heights, PDFs and generalized second-order  
527 structure functions, are used to study the random field of bed elevations, as represented by the  
528 DEMs. The advantages and disadvantages of the three measurement techniques in use are  
529 discussed, as well as their suitability for obtaining DEMs for statistical roughness analysis.

530 The results show that all three measurement techniques used for this study are capable of  
531 recording DEMs with sampling distances small enough to examine an evolving gravel-bed at  
532 the grain scale in laboratory conditions, using a sediment mixture with  $D_{50} = 7$ -mm. Statistical  
533 analysis resulted in describing vertical as well as horizontal roughness characteristics.  
534 Although, visually, differences in the DEMs obtained with different measurement techniques  
535 are observed, the results of the chosen statistical analysis do not disclose the visual differences  
536 to the same extent.

537 The accuracy of the DEM obtained with stereo-photogrammetry in the first part of this study  
538 is inferior to the DEMs obtained with the other techniques, which did not agree with what is  
539 theoretically achievable with a stereo-photogrammetric system. We thus presented changes  
540 made in the setup, resulting in the highest gravel-bed DEM resolution obtained with stereo-  
541 photogrammetry, 25-million points/m<sup>2</sup>. The result warrants further research into setting up  
542 non-proprietary stereo-photogrammetric systems for sediment transport studies. Work is  
543 needed to prepare a gravel-bed ground truth to quantitatively validate the DEM's accuracy  
544 obtained with the non-proprietary stereo-photogrammetric system. The next step is to employ

545 and validate the system underwater, and obtain DEMs to study the dynamic behavior of  
546 gravel-beds at the grain-scale.

## 547 **ACKNOWLEDGEMENTS**

548 Photogrammetric application was conducted in collaboration with the Department of  
549 Computer Science, The University of Auckland. We would like to thank in particular Patrice  
550 Delmas, Alfonso Gastelum Strozzi and Edwin Chan for their valuable input in obtaining the  
551 stereo-photogrammetric data. Laser scanning was undertaken with the help of the Department  
552 of Mechanical Engineering, The University of Auckland. We would like to thank Katherine  
553 Heays, who introduced the first author to the lab environment. The Fluid Mechanics  
554 Laboratory technicians Geoff Kirby and Jim Luo helped in conducting the experiments.

## 555 **REFERENCES**

- 556 Aberle, J., and Nikora, V. (2006). "Statistical properties of armored gravel bed surfaces."  
557 *Water Resour. Res.*, 42, W11414.
- 558 Aberle, J., Nikora, V., Henning, M., Ettmer, B., and Hentschel, B. (2010). "Statistical  
559 characterization of bed roughness due to bed forms: A field study in the Elbe River at  
560 Aken, Germany." *Water Resour. Res.*, 46, W03521.
- 561 Andreas, E. L., and Trevino, G. (1997). "Using wavelets to detect trends." *J. Atmos. Ocean.*  
562 *Tech.*, 14(3), 554-564.
- 563 Bouguet, J.-Y., and Perona, P. (1998). "Camera calibration from points and lines in dual-  
564 space geometry." *Technical report*, California Institute of Technology, 1-16.
- 565 Brasington, J., and Smart, R. M. A. (2003). "Close range digital photogrammetric analysis of  
566 experimental drainage basin evolution." *Earth Surf. Proc. Land.*, 28(3), 231-247.
- 567 Bunte, K., and Abt, S. R. (2001). "Sampling surface and subsurface particle-size distributions  
568 In wadable gravel- and cobble-bed streams for analyses in sediment transport,  
569 hydraulics, and streambed monitoring." *Gen. Tech. Rep. RMRS-GTR-74*, U.S. Dept. of

570 Agriculture, Forest Service, Rocky Mountain Research Station, Fort Collins, CO, 1-  
571 428.

572 Butler, J. B., Lane, S. N., and Chandler, J. H. (1998). "Assessment of DEM quality for  
573 characterizing surface roughness using close range digital photogrammetry."  
574 *Photogramm. Rec.*, 16(92), 271-291.

575 Butler, J. B., Lane, S. N., and Chandler, J. H. (2001). "Characterization of the structure of  
576 river-bed gravels using two-dimensional fractal analysis." *Math. Geol.*, 33(3), 301-  
577 330.

578 Butler, J. B., Lane, S. N., Chandler, J. H., and Porfiri, E. (2002). "Through-water close range  
579 digital photogrammetry in flume and field environments." *Photogramm. Rec.*, 17(99),  
580 419-439.

581 Carbonneau, P. E., Lane, S. N., and Bergeron, N. E. (2003). "Cost-effective non-metric close-  
582 range digital photogrammetry and its application to a study of coarse gravel river  
583 beds." *Int. J. Remote Sens.*, 24(14), 2837–2854.

584 Chandler, J., Shiono, K., Rameshwaran, P., and Lane, S. (2001). "Measuring flume surfaces  
585 for hydraulics research using a Kodak DCS460." *Photogramm. Rec.*, 17(97), 39-61.

586 Chang, F. J., and Chung, C. H. (2012). "Estimation of riverbed grain-size distribution using  
587 image-processing techniques." *J. Hydrol.*, 440-441, 102-112.

588 Clifford, N., Robert, A., and Richards, K. (1992). "Estimation of flow resistance in gravel-  
589 bedded rivers a physical explanation of the multiplier of roughness length." *Earth*  
590 *Surf. Proc. Land.*, 17(2), 111-126.

591 Coleman, S. E. (1997). "Ultrasonic measurement of sediment bed profiles." *Proc.*, 27th  
592 *Congress of the International Association for Hydraulic Research*, San Francisco,  
593 California, USA, 221-226.

594 Cooper, J. R., and Tait, S. J. (2009). "Water-worked gravel beds in laboratory flumes - a  
595 natural analogue?" *Earth Surf. Proc. Land.*, 34(3), 384-397.

596 de Jong, C. (1995). "Temporal and spatial interactions between river bed roughness,  
597 geometry, bedload transport and flow hydraulics in mountain streams - examples from  
598 Squaw Creek (Montana, USA) and Lainbach/Schmiedlaine (Upper Bavaria,  
599 Germany)." Ph.D. thesis, Free University of Berlin, Berlin.

600 Detert, M., and Weitbrecht, V. (2012). "Automatic object detection to analyze the geometry  
601 of gravel grains." *Proc.*, *River Flow 2012*, Taylor and Francis Group, San Jose, Costa  
602 Rica, 6.

603 Fehr, R. (1987). "Geschiebeanalysen in Gebirgsflüssen; Umrechnung und Vergleich von  
604 verschiedenen Analyseverfahren." *Mitteilung Nr. 92 der Versuchsanstalt für*  
605 *Wasserbau, Hydrologie und Glaziologie, Eidgenössischen Technischen Hochschule*  
606 *Zürich.*

607 Friedrich, H. (2010). "Evaluation of statistical analysis techniques for developing bedforms  
608 recorded in 3D." Ph.D. thesis, The University of Auckland, Auckland.

609 Gimel'farb, G. (2002). "Probabilistic regularisation and symmetry in binocular dynamic  
610 programming stereo." *Pattern Recogn. Lett.*, 23(4), 431-442.

611 Goring, D. G., Nikora, V. I., and McEwan, I. K. (1999). "Analysis of the texture of gravel-  
612 beds using 2-D structure functions." *Proc., I.A.H.R. Symposium on River, Coastal and*  
613 *Estuarine Morphodynamics*, Genova, Italy, 111-120.

614 Graham, D. J., Rollet, A. J., Piégay, H., and Rice, S. P. (2010). "Maximizing the accuracy of  
615 image-based surface sediment sampling techniques." *Water Resour. Res.*, 46(2), 15.

616 Heritage, G., and Hetherington, D. (2007). "Towards a protocol for laser scanning in fluvial  
617 geomorphology." *Earth Surf. Proc. Land.*, 32(1), 66-74.

618 Hodge, R., Brasington, J., and Richards, K. (2008). "In situ characterization of grain-scale  
619 fluvial morphology using Terrestrial Laser Scanning." *Earth Surf. Proc. Land.*, 34(7),  
620 954-968.

621 Hodge, R., Brasington, J., and Richards, K. (2009). "Analysing laser scanned digital terrain  
622 models of gravel bed surfaces: linking morphology to sediment transport processes  
623 and hydraulics." *Sedimentology*, 56(7), 2024-2043.

624 Lane, S. N., Richards, K. S., and Chandler, J. H. (1994). "Developments in monitoring and  
625 modelling small-scale river bed topography." *Earth Surf. Proc. Land.*, 19(4), 349-368.

626 Nikora, V. I., Goring, D. G., and Biggs, B. J. F. (1998). "On gravel-bed roughness  
627 characterization." *Water Resour. Res.*, 34(3), 517-527.

628 Rapp, C., Eder, K., and Stilla, U. (2012). "3D determination of the evolution of a scour hole  
629 by photogrammetric means." *Proc., River Flow 2012*, Taylor & Francis Group, San  
630 Jose, Costa Rica, 943-950.

631 Robert, A. (1988). "Statistical properties of sediment bed profiles in alluvial channels." *Math.*  
632 *Geol.*, 20(3), 205-225.

633 Robert, A. (1990). "Boundary roughness in coarse-grained channels." *Prog. Phys. Geog.*,  
634 14(1), 42-70.

635 Robert, A., and Richards, K. S. (1988). "On the modelling of sand bedforms using the  
636 semivariogram." *Earth Surf. Proc. Land.*, 13(5), 459-473.

637 Smart, G., Aberle, J., Duncan, M., and Walsh, J. (2004). "Measurement and analysis of  
638 alluvial bed roughness." *J. Hydraul. Res.*, 42(3), 227-237.

639 Strom, K. B., Kuhns, R. D., and Lucas, H. J. (2010). "Comparison of automated image-based  
640 grain sizing to standard pebble-count methods." *J. Hydraul. Eng.*, 136(8), 461-473.

641 Westaway, R. M., Lane, S. N., and Hicks, D. M. (2000). "The development of an automated  
642 correction procedure for digital photogrammetry for the study of wide, shallow,  
643 gravel-bed rivers." *Earth Surf. Proc. Land.*, 25(2), 209-226.

644 Westaway, R. M., Lane, S. N., and Hicks, D. M. (2001). "Remote sensing of clear-water,  
645 shallow, gravel-bed rivers using digital photogrammetry." *Photogramm. Eng. Rem. S.*,  
646 67(11), 1271-1281.

647 Wolman, M. G. (1954). "A Method of Sampling Coarse River-Bed Material." *Transactions,*  
648 *American Geophysical Union*, 35(6).

649 Zhang, Z. (1998). "A Flexible New Technique for Camera Calibration." *IEEE T. Pattern*  
650 *Anal.*, 22(11), 1330-1334.

651

652

653

**Table 1 Summary of the measurement specifications.**

<i>Measurement technique</i> <i>Measurement specifications</i>	<b>Acoustic bed-profiler</b>	<b>Laser-scanner</b>	<b>Stereo-photogrammetric setup (first part)</b>	<b>Improved stereo-photogrammetric setup (second part)</b>
<b>[Downstream x transverse] DEM sampling distance (mm)</b>	2.45 x 2.54	1.45 x 1.45	1 x 1	0.2 x 0.2
<b>Theoretical vertical accuracy (mm)</b>	0.37	0.05	1	0.34

654

655

656

657

658

659

660

661

662

663

664 **Table 2 Texture coefficients extracted from bed elevation PDFs and structure functions.**

<i>Bed condition</i>	<b>Screeded bed</b>	<b>Water-worked bed</b>			
<i>Measurement technique</i>	<b>Acoustic bed-profiler</b>	<b>Acoustic bed-profiler</b>	<b>Laser-Scanner</b>		<b>Stereo-Photogrammetry</b>
<i>Bed condition</i> <i>Texture coefficients</i>	<b>Submerged</b>	<b>Submerged</b>	<b>Dry surface</b>	<b>Wet surface</b>	<b>Dry surface</b>
<b>Skewness (-)</b>	-0.5	0.81	0.79	0.86	0.5
<b>Kurtosis (-)</b>	4.57	3.8	4.07	4.26	3.58
<b><math>\sigma_z</math> (mm)</b>	1.33	5.76	5.32	5.32	5.0
<b><math>\Delta x_0</math> (mm)</b>	6	7.2	9.7	10.1	6.9
<b><math>\Delta y_0</math> (mm)</b>	6.8	8.5	8	8.1	9

665